



Enhancement of visible-light-driven photocatalytic H₂ evolution from water over g-C₃N₄ through combination with perylene diimide aggregates

Shuai Chen ^{a,b}, Chen Wang ^c, Benjamin R. Bunes ^c, Yingxuan Li ^a, Chuanyi Wang ^{a,*}, Ling Zang ^{c,*}

^a Laboratory of Environmental Sciences and Technology, Xinjiang Technical Institute of Physics & Chemistry, Key Laboratory of Functional Materials and Devices for Special Environments, Chinese Academy of Sciences, Urumqi, 830011, China

^b The Graduate School of Chinese Academy of Science, Beijing, 100049, China

^c Nano Institute of Utah and Department of Materials Science and Engineering, University of Utah, Salt Lake City, UT, 84112, USA



ARTICLE INFO

Article history:

Received 29 January 2015

Received in revised form 18 March 2015

Accepted 19 March 2015

Available online 28 March 2015

Keywords:

Photocatalysis

Water-splitting

Hydrogen

g-C₃N₄

Perylene diimide

ABSTRACT

Graphitic carbon nitride (g-C₃N₄) is among the most promising metal-free photocatalysts for H₂ production from solar-driven water reduction. However, the photocatalytic efficiency of bulk g-C₃N₄ powders is limited. In this work, molecular aggregates of perylene tetracarboxylic diimides (PTCDIs, a robust class of air-stable n-type organic semiconductor) were loaded via solution processing on the surface of g-C₃N₄, which is pre-deposited with cocatalyst Pt nanoparticles. The PTCDIs/Pt/g-C₃N₄ composites thus fabricated exhibit broader visible-light response than Pt/g-C₃N₄, and possess excellent photochemical stability. The initial intramolecular charge transfer features of the PTCDIs, as well as their energy levels being matched to g-C₃N₄, ensure subsequent charge separation in the PTCDIs/Pt/g-C₃N₄ composites. When the composites are dispersed into aqueous solutions containing triethanolamine as a sacrificial electron donor, a tenfold enhancement of H₂ evolution activity ($\sim 0.375 \mu\text{mol h}^{-1}$) is achieved compared to bare Pt/g-C₃N₄ under visible-light ($\lambda \geq 420 \text{ nm}$) irradiation.

© 2015 Elsevier B.V. All rights reserved.

1. Introduction

Hydrogen (H₂) is an ideal green energy source to alleviate the impact of fossil fuel scarcity and environmental risk because it is renewable, energy dense, and environmentally friendly [1]. Splitting water using a photocatalytic reduction reaction on a semiconductor surface utilizing abundant solar energy has been demonstrated as a promising approach for clean, cost-effective production of H₂ [2–4]. In contrast to most inorganic semiconductor photocatalysts, metal-free polymeric graphitic carbon nitride, g-C₃N₄, is an inexpensive, effective, and photochemically stable organic semiconducting photocatalyst for H₂ generation from water reduction [5–7]. Related work originates from Wang's pioneering work in 2009 and has attracted intense interest in subsequent years, yielding a great deal of promising results [7,8]. However, despite its appealing features, the photocatalytic activity of bare g-C₃N₄ is relatively unsatisfied [9,10]. There are three main reasons for the unsatisfactory efficiency of as-prepared bulk

g-C₃N₄ powders: (1) limited utilization of visible-light due to its moderate bandgap ($E_g = \sim 2.7 \text{ eV}$, corresponding to an optical wavelength of $\sim 460 \text{ nm}$); (2) rapid recombination of photoinduced electrons and holes due to the unavoidably disordered structure or defects; and (3) relatively small Brunauer–Emmett–Teller (BET) surface area (normally below $10 \text{ m}^2 \text{ g}^{-1}$) [7,10]. Consequently, many attempts have been made to improve the photocatalytic performance. Combination of g-C₃N₄ with dye molecules may improve their visible-light response via sensitization process [7,8]. Normally, Pt nanoparticles are loaded onto the surface of g-C₃N₄ matrix to enhance their photocatalytic water reduction efficiency as cocatalyst [10]. Additionally, the presence of sacrificial electron donors, such as triethanolamine, methanol and ethylenediaminetetraacetic acid, is often necessary for photocatalytic H₂ production from water [7]. To enlarge the BET surface of g-C₃N₄, various micro/nanostructures (like nanoporous, nanosheet, etc.) have been constructed via different fabrication methods [7,10]. The morphologies are highly affected by factors such as precursors, condensation temperatures, and complex fabrication processes [7,10]. Thereby, bulk-phase g-C₃N₄ is still a representative good candidate to study the photosensitizing action of dyes.

* Corresponding authors. Tel.: +86 991 3835879; fax: +86 991 3838957.

E-mail addresses: cwyang@ms.xjb.ac.cn (C. Wang), lzang@eng.utah.edu (L. Zang).

For visible-light-driven H₂ production, dyes with or without metals, such as ruthenium(II) complexes, nickel-thiourea-triethylamine complex, magnesium phthalocyanine, Eosin Y, and Erythrosin B, have been used as sensitizers for g-C₃N₄ [11–15]. These dyes suffer from disadvantages such as requiring expensive rare earth elements, poor stability under light irradiation or in water, limited visible-light response, complicated synthesis, or difficult functionalization. Therefore, their practical applications are limited [2–4]. In contrast, perylene tetracarboxylic diimides (PTCDIs), a robust class of air-stable n-type organic semiconductor molecules, exhibit high thermal and photostability, and strong light absorption (nearly covering the whole visible light spectrum) [16,17]. With suitable structural modification and the planar π-conjugate structure, PTCDIs can be fabricated into photoactive semiconductor heterostructures [17–20]. These features make PTCDIs strong candidates for light harvesting sensitizers in dye-sensitized photochemical systems. In fact, such applications have achieved enormous attention in organic photovoltaic fields, as well as TiO₂-based photo-degradation of pollutants [20–23]. On the other hand, PTCDIs solid owns an appropriate band structure, which encompasses the reduction and oxidation potentials of water [4,17]. However, the applicability of PTCDIs in photocatalytic H₂ production field is seldom reported. The main obstacles are considered to be their electron-deficient π-conjugated cores, rapid charge recombination, and inefficient charge transport in disorder molecular system [2,20,23].

However, large exciton diffusion lengths and high electron mobility of PTCDIs can be achieved through the extended π–π electronic interaction enabled by the cofacial molecular stacking [17]. Significant efforts have focused on designing intramolecular electron donor–acceptor structures and constructing orderly, one-dimensional (1D) nanostructures of PTCDIs (e.g., nanofiber) via self-assembly driven by strong π–π stacking of their large planar aromatic cores [21,22,24]. In 2010, Zang's group reported that an electron-rich dimethylaminobenzyl group attached to the imide-position of the PTCDIs molecule can facilitate intramolecular charge separation under visible-light irradiation. Meanwhile, efficient charge transport was achieved along long axis of nanofibers under white light [19]. Inspired by this, we have recently demonstrated the applicability of a series of PTCDI nanofiber composites for photocatalytic H₂ production from water reduction [25]. Meanwhile, a similar photocatalytic concept was also proven for the nanofibers of perylene monoimides [26].

In this work, we reported on a novel visible-light-driven composite photocatalyst employing g-C₃N₄ as the matrix and PTCDIs assembles as the adjuncts (Fig. 1). g-C₃N₄ was prepared from one-step thermal condensation of a cheap and abundant precursor, melamine. Symmetric PTCDI-1 and asymmetric PTCDI-2 molecules modified with 4-dimethylaminobenzyl and/or dodecyl side groups were synthesized to explore the effect of side-chain modification on aggregation behaviour, nanostructure morphology and photocatalytic activity. After photo-deposition of Pt on g-C₃N₄, a bisolvent-exchange triggered aggregation method [27]

was used to prepare PTCDI/Pt/g-C₃N₄ composites. Then, the composite particles were suspended in aqueous solutions containing triethanolamine (sacrificial electron donor) to sustain the photocatalytic reaction under visible-light illumination. For comparison, the photocatalytic activity of Pt/g-C₃N₄ as well as Pt/PTCDIs nanofiber composites was also investigated to help understand the improved photocatalytic activity of PTCDI/Pt/g-C₃N₄ composites.

2. Experimental

2.1. Preparation of materials

Bulk g-C₃N₄ powders (Fig. 2a) used in this study were prepared using simple pyrolysis technique through thermal polycondensation of melamine at 600 °C for 4 h under ambient pressure in air [7,8,28]. g-C₃N₄ thus prepared contains structural defects such as =NH, –NH₂, and –OH groups which can be attributed to imperfect condensation and adsorbed H₂O [10,29,30]. The resultant brown–yellow powder was collected, ground and used as the photocatalyst matrix without any further treatment. Pt as a cocatalyst for photocatalytic H₂ evolution was loaded onto the g-C₃N₄ powders via a typical and simple in situ photoreduction procedure from an aqueous solution of H₂PtCl₆·6H₂O [25]. The greyish yellow powder Pt/g-C₃N₄ (Fig. 2b) was ground and used as sensitization matrix for the following test without further treatment. The synthesis of symmetric PTCDI-1 (Fig. 2c) and asymmetric PTCDI-2 (Fig. 2d) was performed following a typical Langals' procedure with yields of ca. 80% and 45%, respectively, that is, by condensation of commercially available perylene 3,4,9,10-tetracarboxylic dianhydride (PTCDA) with 4-(dimethylamino)benzylamine and/or dodecylamine in molten imidazole under a N₂ protection [17,19].

2.2. Preparation of PTCDIs/Pt/g-C₃N₄ composites

10 mL of PTCDIs solution in CHCl₃ (125 mg L^{−1}) was mixed with ground Pt/g-C₃N₄ fine powders (25 mg) in a 100 mL round-bottom flask. The mixtures were ultrasonicated and stirred at 25 °C for 6 h in the dark, and then another 2 h after the injection of 40 mL of CH₃OH dropwise. The precipitates were collected by vacuum suction filtration using 0.45 μm membrane filter and then dried at 80 °C for 6 h to give PTCDI-1/Pt/C₃N₄ (Fig. 2e) and PTCDI-2/Pt/C₃N₄ powders (Fig. 2f). Comparatively, 1D self-assembly of PTCDIs nanofibers were performed via feasible bisolvent phase-transfer process by injecting a large amount of CH₃OH (400 mL) into concentrated CHCl₃ (100 mL; 400 μmol L^{−1}) solutions of PTCDIs [19,25]. Then, Pt (0.5 wt.%) was deposited on PTCDIs nanofibers (denoted as Pt/PTCDIs) following the same in situ photo-reduction process just as above described to prepare Pt/g-C₃N₄.

2.3. Characterization

Thermogravimetry analysis (TGA) of PTCDIs was performed on a NETZSCH STA 449F3 instrument. The samples were heated in an

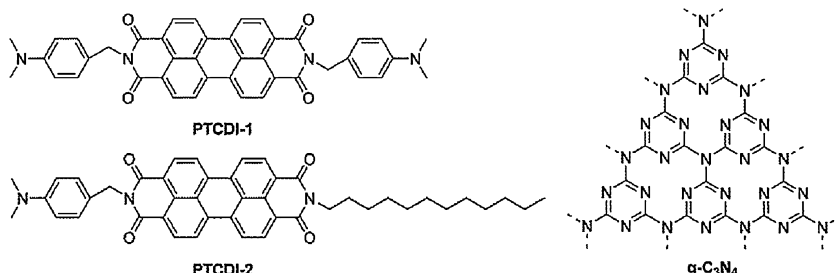


Fig. 1. Chemical structures of PTCDI-1 and PTCDI-2 molecules, and g-C₃N₄.



Fig. 2. Photo images of (a) $\text{g-C}_3\text{N}_4$, (b) Pt/ $\text{g-C}_3\text{N}_4$, (c) PTCDI-1, (d) PTCDI-2, (e) PTCDI-1/Pt/ $\text{g-C}_3\text{N}_4$ and (f) PTCDI-2/Pt/ $\text{g-C}_3\text{N}_4$.

alumina crucible in the range from room temperature to 800 °C with a heating rate of 10 °C min⁻¹ under air atmosphere. UV-vis diffused reflectance spectra (DRS) of the samples was recorded at room temperature on an EVOLUTION 220 UV-vis spectrophotometer equipped with an integrating sphere assembly. Scanning electron microscopy (SEM) images were obtained on a ZEISS SUPRA55VP microscope. Specific surface areas of samples were measured by the BET method (N_2 adsorption) in a N_2 adsorption apparatus (Quantachrome 1900 Corporate Drive). Photographs were taken with a Canon IXUS 155. Cyclic voltammetry (CV) measurements were performed in a conventional three-electrode cell with Pt wires with diameters of 1 mm as the working and counter electrodes, while an Ag/AgCl electrode served as the reference electrode [27]. The electrodes were directly immersed in the solution containing a solution of PTCDIs (5 mmol L⁻¹) in dry CH₃CN in the presence of tetra-n-butylammonium hexafluorophosphate (0.1 mmol L⁻¹) using a Model 263A workstation (EG&G Princeton Applied Research). Tests were carried out at a scan rate of 50 mV s⁻¹ at 25 °C under nitrogen protection. For electrochemical characterization of the solids, the working electrodes were prepared by a dispersing process. Typically, the methanol slurries of $\text{g-C}_3\text{N}_4$ or Pt/ $\text{g-C}_3\text{N}_4$ were carefully dropped down onto pre-cleaned indium tin oxide (ITO) glass substrates and then flattened. The ITO electrodes were dried in air and annealed at 100 °C for 2 h.

2.4. Photocatalytic tests

H_2 generation experiments were carried out in a top-irradiation type reactor connected to a closed gas circulation and evacuation system (Labsolar-H₂ photocatalytic water-splitting H₂ production system, Bofeilai, Beijing). Generally, 25 mg of the photocatalyst powder was suspended using a magnetic stirrer in 100 mL aqueous solution containing triethanolamine (10 vol.%) as sacrificial electron donor. Before photo-irradiation, the system was evacuated several times to remove oxygen, and the reaction temperature

was maintained at 25 °C by a flow of cooling water during the entire experiment. A 400 W Xenon lamp (CEL-S500, Beijing AULT) attaching with a 420 nm cutoff optical filter was used as the light source. The distance between the light source and the liquid level in the reactor is 10 cm. The effective irradiation surface area is 19.6 cm². The intensity of the incident light (>420 nm) was measured to be $0.15 \pm 0.02 \text{ W cm}^{-2}$ with an optical power metre (NEWPORT 1916-C). The amount of evolved H₂ was detected and analyzed by an inline gas chromatography (GC-system 7890A; Agilent Technologies) with N₂ as the carrier gas. The apparent quantum efficiency (AQE) measurement was carried out under the similar photocatalytic reaction conditions only with 0.3 g catalysts and irradiation light at 420 nm by using combined band-pass filter (full width at half maxima is 15 nm). The irradiated light intensity of 420 nm was measured to be ca. 20 mW cm⁻². AQE is estimated according to a typical equation,

$$\text{AQE} = \frac{2(\text{number of evolved hydrogen molecules})}{(\text{number of incident photons})} \times 100\% \\ = \frac{2ntN}{EAt\lambda/hc} \times 100\%$$

where n is the amount of H₂ evolution under the light with the wavelength λ , t is the illumination time, N is Avogadro constant, E is the irradiated light intensity, A is the effective irradiation surface area, h is the Planck constant, and c is the speed of light.

3. Results and discussion

3.1. Materials and characterization

Their morphology with amorphous structure of $\text{g-C}_3\text{N}_4$ was indicated by SEM characterization (Fig. 3a). The mesoporous skeleton and structural defects such as $=\text{NH}$, $-\text{NH}_2$ and $-\text{OH}$ of $\text{g-C}_3\text{N}_4$ thus prepared facilitate the surface binding of Pt cocatalysts [29,30]. Moreover, these moieties can bind with the two PTCDIs

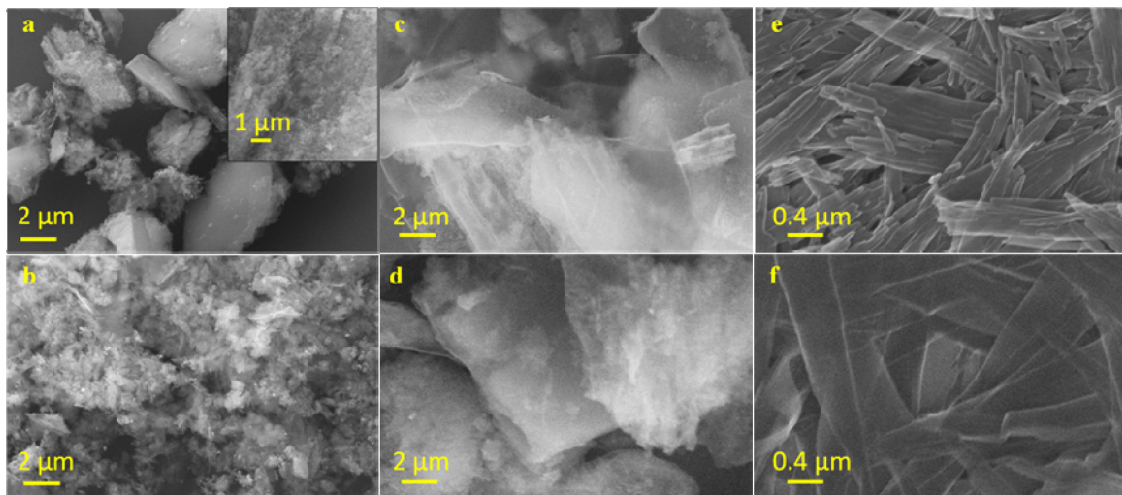


Fig. 3. SEM images of (a) $\text{g-C}_3\text{N}_4$ and its microtopography (inset), (b) Pt/ $\text{g-C}_3\text{N}_4$, (c) PTCDI-1/Pt/ $\text{g-C}_3\text{N}_4$, (d) PTCDI-2/Pt/ $\text{g-C}_3\text{N}_4$, (e) PTCDI-1 nanofibers and (f) PTCDI-2 nanofibers fabricated individually via self-assembly.

Table 1

Forniter molecular orbital energies of PTCDIs, g-C₃N₄ and Pt/g-C₃N₄ estimated from electrochemical CV measurements.

Sample	<i>E</i> _{ox} /eV	<i>E</i> _{red} /eV	<i>E</i> _{HOMO} /eV	<i>E</i> _{LUMO} /eV	Bandgap/eV
PTCDI-1	1.85	−0.87	−6.35	−3.63	2.72
PTCDI-2	1.84	−0.76	−6.34	−3.74	2.60
g-C ₃ N ₄	2.25	−0.73	−6.75	−3.77	2.98
Pt/g-C ₃ N ₄	2.23	−0.72	−6.73	−3.78	2.95

Note: HOMO and LUMO values were calculated using the equation. $E_{\text{HOMO}} = -4.5 \text{ eV} - E_{\text{ox}}$; $E_{\text{LUMO}} = -4.5 \text{ eV} - E_{\text{red}}$.

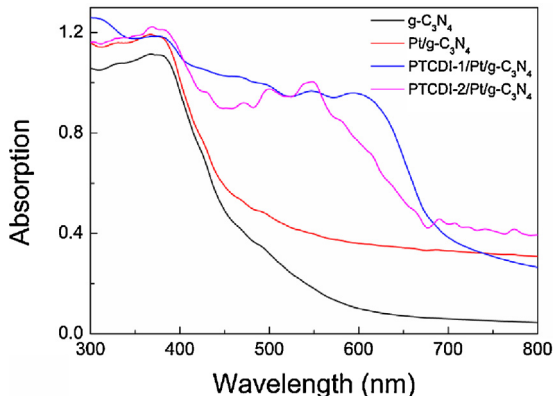


Fig. 4. DRS absorption spectra of g-C₃N₄, Pt/g-C₃N₄ and PTCDIs/Pt/g-C₃N₄ composites.

(Fig. 1) through hydrogen bonding, which in conjunction with $\pi-\pi$ interaction would enforce a strong contact (tight junction) between PTCDI and g-C₃N₄, thus enhancing the interfacial electron transfer (vide infra) [31]. Consistent with the colour change from yellow g-C₃N₄ (Fig. 2a) to greyish Pt/g-C₃N₄ (Fig. 2b), well-dispersion of Pt nanoparticles on the surface of g-C₃N₄ is also revealed by SEM (Fig. 3) images and demonstrated by DRS spectra (Fig. 4), where Pt/g-C₃N₄ exhibits a small red-shift of the absorption band-edge [10]. Consequently, Pt/g-C₃N₄ possesses a slightly narrower bandgap ca. 2.95 eV from the onset of the DRS spectrum, which is sufficient for its use in water reduction reaction, which requires 1.23 eV theoretically [2]. The bandgap was also indicated by the electrochemical CV measurement as shown in Table 1. In addition to the appropriate energy levels, a large surface area of photocatalyst is also required for efficient H₂ evolution [31]. BET analysis revealed such g-C₃N₄ powders is approximately 35 m² g⁻¹ (Fig. S1), larger than that of common bulk g-C₃N₄ (<10 m² g⁻¹), mainly due to the influence of temperature and air atmosphere [13]. The porosity of these powders containing small mesopores about 3.8 nm in diameter was demonstrated using N₂ adsorption–desorption isotherms at liquid nitrogen temperature. In general, a larger surface area offers more surface sites for PTCDI adsorption, leading to enhanced light-harvesting, and the mesoporous structure shortens the diffusion path of free carriers from the bulk to the surface resulting into increased photoactivity [13,30].

Key design criteria in developing an ideal photocatalytic system include efficient visible-light harvesting, effective interfacial charge transfer (here specifically between PTCDI and g-C₃N₄) and suppression of recombination of the photogenerated electrons and holes [25,32,33]. The electron-rich (dimethylamino)benzyl moiety was added to the electron-deficient PTCDI unit to construct a donor-acceptor structure in both two PTCDI derivatives (denoted as PTCDI-1 and PTCDI-2, Fig. 1) to enable photoinduced intramolecular charge transfer [19]. Additionally, the dodecyl modification was implemented to tune the intramolecular charge separation and effect on the photocatalytic activity of PTCDIs [24]. Moreover, there is an additional methyl space between the (dimethylamino)phenyl

group and PTCDI core, which enables more efficient intramolecular charge separation under illumination [19]. This property should contribute to the increased photocatalytic activity as to be discussed later. Both PTCDI-1 and PTCDI-2 exhibit remarkable thermodynamic stability under air atmosphere as shown in Fig. S2, and broadened and strong optical absorption in the visible light region in the solid state (Fig. S3) in accordance to their dark-red (Fig. 2c) or red (Fig. 2d) colour. The strong visible absorption, together with the LUMO positions and bandgaps as listed in Table 1, implies high promise of these PTCDIs for water reduction applications utilizing visible-light [3,7]. Further, the existence of two electron-rich aromatic groups increases the reduction potential of PTCDI-1, and thus elevates its LUMO level. Additionally, in respect to the presence of nodes at the N- and N'-positions of PTCDI structure, PTCDI-1 and PTCDI-2 exhibit similar strong absorption in the visible light region (Fig. S3). As a result, the comparison of photocatalytic activity between them and following PTCDIs/Pt/g-C₃N₄ composites arising from side-group functionalization becomes convenient.

3.2. Construction of nanocomposites

To realize a functional photocatalytic system, PTCDIs/Pt/g-C₃N₄ composites (Fig. 2e and f) composed of PTCDI aggregates on the Pt/g-C₃N₄ matrix were fabricated. It is known that the organization of molecules into ordered assemblies provides continuous pathway for charge transport [24]. Inspired by the reported self-assembly strategy [24], a quick injection and dispersion method was initially introduced to prepare PTCDIs/Pt/g-C₃N₄ composites. As shown in Fig. 3c and d, PTCDI-1 and PTCDI-2 adsorb on the surface of the Pt/g-C₃N₄, creating a layer-like morphology via hydrogen bonding and $\pi-\pi$ stacking in the presence of two different solvents, CHCl₃ (good)/CH₃OH (poor). This method has the advantages of low-cost, low power consumption, easy scaling, and simplicity [36]. As can be seen from the DRS results (Fig. 4), the absorption edge of Pt/g-C₃N₄ shifts towards longer wavelengths (up to 700 nm) in the visible range after combination with PTCDIs, which makes the PTCDIs/Pt/g-C₃N₄ composites strong candidates for visible-light-driven photocatalysts.

3.3. Nanoscale self-assembly

To evaluate the photocatalytic water reduction activity of PTCDIs alone, nanofibers of PTCDIs were fabricated through solution phase self-assembly performed via a simple bisolvent interfacial transfer process, as established in previous reports [25,34]. 1D self-assembly of PTCDIs occurs because of their decreasing solubility when injecting a larger volume of CH₃OH into their CHCl₃ solution at a 4:1 volume ratio. The insolubility drives the strong intrinsic co-facial $\pi-\pi$ stacking of the aromatic core (stacking along the long axis) in conjunction with the association between the side chains (aggregating along the short axis) [19,35]. SEM images (Fig. 3e) show the symmetric PTCDI-1 formed short, narrow nanobelts, likely attributed to its non-coplanar side chain modification. In comparison, longer, thinner nanobelts were obtained from asymmetric PTCDI-2 (Fig. 3f), likely due to the more flexible tuning of molecular stacking by the linear alkyl chain on one side

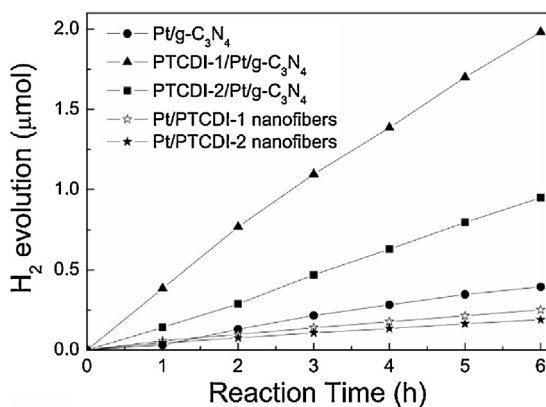


Fig. 5. The time courses of H₂ evolution from water over Pt/g-C₃N₄, PTCDIs/Pt/g-C₃N₄ and Pt/PTCDIs nanofibers.

[25]. Despite the different morphologies, both PTCDI nanostructures form extended 1D charge carrier pathways (enabled by the π–π stacking) and have large surface area, making them appropriate for comparative photocatalytic investigation.

3.4. Photocatalytic H₂ production

Photocatalytic H₂ evolution reactions were performed in aqueous solutions with 10% (by volume) triethanolamine as the sacrificial electron donor under visible-light ($\lambda \geq 420$ nm) illumination. As shown in Fig. 5, steady H₂ evolution from the PTCDI/Pt/g-C₃N₄ systems are observed with production rate up to 0.375 μmol h⁻¹ obtained for PTCDI-1/Pt/g-C₃N₄, which is about ten times higher than that of Pt/g-C₃N₄. Furthermore, Pt/PTCDI nanofibers without the g-C₃N₄ showed much lower activity (ca. 0.0225–0.0375 μmol h⁻¹, Fig. 5) under the same conditions, owing to the intrinsic inefficient photoactivity of organic dyes without a semiconductor matrix to act as an efficient charge separator [2]. Thus, a synergistic role is identified for PTCDIs and g-C₃N₄. In principle, the mesoporous morphology of g-C₃N₄ facilitates the surface deposition of PTCDI (and thus the charge separation), and mass diffusion during the photocatalytic H₂ evolution reactions [7]. Nevertheless, in both cases, composites containing symmetric dimethylamino)benzyl substituted PTCDI-1 give rise to improved photocatalytic activity arising from enhanced intramolecular charge separation (due to two electron donor groups) and higher LUMO orbital than that of asymmetric PTCDI-2. Such intramolecular charge transfer can be also observed from Fig. S4, where neither PTCDI-1 nor PTCDI-2 has fluorescence emission at white or UV light, demonstrating efficient photoinduced intermolecular charge transfer within the π–π assemblies, which is consistent with the H₂ evolution capabilities of Pt/PTCDI nanofibers [25]. Moreover, as summarized in Table 2, under the irradiation of monochromatic light with the wavelength of 420 nm, the AQEs of different photocatalysts are ranked as PTCDI/Pt/g-C₃N₄ > Pt/g-C₃N₄ > Pt/PTCDI nanofiber. PTCDI-1/Pt/g-C₃N₄ shows the highest activity, which is about sevenfold higher than that of Pt/g-C₃N₄ and

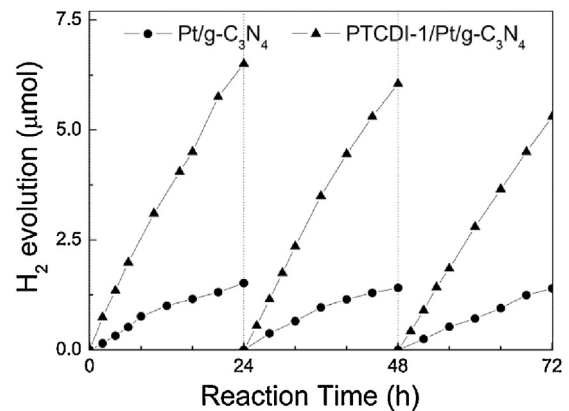


Fig. 6. Stable H₂ evolution from water at PTCDI-1/Pt/g-C₃N₄. The reaction was continued for 72 h, and reset every 24 h.

tenfold higher than that of Pt/PTCDI-1 nanofiber. These AQE data are quite consistent with the photocatalytic H₂ evolution results.

Fig. 6 shows the stability of the photocatalytic activity of PTCDI-1/Pt/g-C₃N₄ for H₂ generation under visible-light illumination. As both PTCDI-1 and g-C₃N₄ are stable under light irradiation in aqueous triethanolamine solutions [37], the photocatalytic reaction results in a stable H₂ evolution rate, although there is still about 20% decrease during 72 h probably due to separation between PTCDI and g-C₃N₄ from stirring. Furthermore, while many dyes suffer from photobleaching [14], PTCDI-1 and PTCDI-2 are stable. They can be regenerated by dissolving the reacted composite powders in CHCl₃. Indeed, reused PTCDI-1/Pt/g-C₃N₄ displayed an equivalent photocatalytic H₂ evolution rate (Fig. S5).

3.5. Tentative mechanism

A “cooperative excitation process” is proposed to explain the photo-induced charge transfer process that enhances H₂ evolution over PTCDI/Pt/g-C₃N₄ compared to bare Pt/g-C₃N₄ or Pt/PTCDIs. As shown in Fig. 7, under visible-light ($\lambda \geq 420$ nm) illumination, both PTCDI and g-C₃N₄ can be excited by absorbing photons. On one hand, an ultra-fast intramolecular charge transfer occurred; that is, after the visible-light-driven excitation of PTCDI, electrons are transferred from the (dimethylamino)benzyl moiety (donor part) to the HOMO orbital of the PTCDI core (acceptor part). Due to the presence of large excess of triethanolamine (sacrificial reagent), the (dimethylamino)benzyl moiety under the oxidation state can be easily reduced to its ground state, thus preventing the charge recombination, leaving excited electrons at the LUMO of PTCDI core. The anionic radical of PTCDI thus formed acts a strong electron donor. On the other hand, the g-C₃N₄ is also excited to promote photo-excited electrons to its conduction band (CB), leaving holes on its valence band (VB). The latter can be quenched by the electrons transferred from the PTCDI's LUMO due to their large energy level difference (driving force). This process inhibits the recombination of photogenerated electron–hole pairs within g-C₃N₄. It should be noted that although the electrons transfer from the LUMO of the PTCDI to the CB of g-C₃N₄ is possible, the process is quite weaken due to the small energy level difference (~0.1 eV). Thus, the collected electrons in the CB of g-C₃N₄ are captured by the loaded cocatalyst Pt nanoparticles, which provide active sites for the reduction of water to H₂ and suppress electron–hole recombination [10]. The electrons are consumed by H₂O to complete the reduction reaction process for H₂ production. Consequently, efficient photoinduced charge separation is achieved both within PTCDI aggregates (via intramolecular electron transfer) and at the interface between PTCDI and g-C₃N₄ (via interfacial electron

Table 2

The data of the apparent quantum efficiency of various photocatalysts.

Photocatalysts	H ₂ evolution rate/μmol h ⁻¹	AQE/%
Pt/PTCDI-1 nanofiber	0.3	0.024
Pt/PTCDI-2 nanofiber	0.25	0.020
Pt/g-C ₃ N ₄	0.6	0.048
PTCDI-1/Pt/g-C ₃ N ₄	3.8	0.31
PTCDI-2/Pt/g-C ₃ N ₄	2.2	0.17

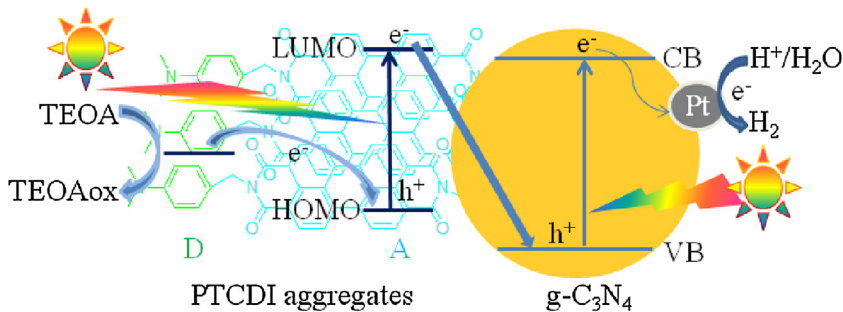


Fig. 7. Proposed mechanism for photocatalytic H_2 evolution over PTCDI/Pt/g-C₃N₄ under visible-light ($\lambda \geq 420$ nm). D: 4-dimethylaminobenzyl moiety of PTCDI; A: perylene core of PTCDI; TEOA: triethanolamine.

transfer). As a result, the PTCDI/Pt/g-C₃N₄ composite photocatalysts exhibit a cooperative effect showing a significantly higher H_2 production than either Pt/g-C₃N₄ or Pt/PTCDI nanofibers. This cooperative behaviour is also demonstrated by the results in Fig. S6, which investigates on the effect of the incident light with different wavelengths on the amount of H_2 evolution. Under irradiation of light with a wavelength of 550 nm (which excites only PTCDIs), the H_2 evolution rate is quite low. It is seen that PTCDI aggregates act as light-sensitizers and provide electron transport for photocatalytic H_2 production from water [33]. Ordered π - π stacking of PTCDI molecules on the surface of π -conjugated g-C₃N₄ further enhances the intra-/inter-molecular charge transfer and separation, which inhibits the rapid recombination of photoinduced electrons and holes in PTCDIs/Pt/g-C₃N₄ composites.

4. Conclusions

To summarize, a PTCDI-1/Pt/g-C₃N₄ composite is demonstrated as an efficient photocatalyst for visible-light-driven photocatalytic water reduction for H_2 evolution. The electron donor-acceptor feature of PTCDI-1 resulting from the presence of electron-rich 4-dimethylaminobenzyl moieties and the π -stacking morphology is expected to play critical roles for the application of PTCDIs in this area. Because of their organic characteristics, strong visible-light response, good stability, economically viability through low-cost scaling, flexible structural designs, and H_2 generation activity, photocatalyst composites of PTCDIs and g-C₃N₄ hold great potential for practical applications in the future. More effort in future will be spent in tuning electron donor-acceptor structure of PTCDI molecules, or introducing functional groups attached to PTCDI molecules that improve anchoring on the matrix of g-C₃N₄ which has much regular morphologies, especially, crystalline nanosheets or porous nanostructures with large surface area.

Acknowledgements

Financial support by the National Natural Science Foundation of China (Grant No. 21173261), the “One Hundred Talents” programme of Chinese Academy of Sciences (Grant No. 1029471301), and the “Cross Cooperation Program for Creative Research Teams” of Chinese Academy of Sciences (Grant No. Y251821601) are gratefully acknowledged.

Appendix A. Supplementary data

Supplementary data associated with this article can be found, in the online version, at <http://dx.doi.org/10.1016/j.apcata.2015.03.026>.

References

- [1] J.R. McKone, N.S. Lewis, H.B. Gray, Chem. Mater. 26 (2014) 407–414.
- [2] M. Ni, M.K.H. Leung, D.Y.C. Leung, K. Sumathy, Renew. Sust. Energ. Rev. 11 (2007) 401–425.
- [3] X.B. Chen, S.H. Shen, L.J. Guo, S.S. Mao, Chem. Rev. 110 (2010) 6503–6570.
- [4] A.A. Ismail, D.W. Bahnemann, Sol. Energy Mater. Sol. Cells 128 (2014) 85–101.
- [5] N. Serpone, A.V. Emeline, J. Phys. Chem. Lett. 3 (2012) 673–677.
- [6] W.J. Youngblood, S.H.A. Lee, K. Maeda, T.E. Mallouk, Acc. Chem. Res. 42 (2009) 1966–1973.
- [7] S.W. Cao, J.G. Yu, J. Phys. Chem. Lett. 5 (2014) 2101–2107.
- [8] X.C. Wang, K. Maeda, A. Thomas, K. Takanabe, G. Xin, J.M. Carlsson, K. Domen, M. Antonietti, Nat. Mater. 8 (2009) 76–80.
- [9] A. Thomas, A. Fischer, F. Goettmann, M. Antonietti, J.O. Müller, R. Schlögl, J.M. Carlsson, J. Mater. Chem. 18 (2008) 4893–4908.
- [10] X.C. Wang, S. Blechert, M. Antonietti, ACS Catal. 2 (2012) 1596–1606.
- [11] K. Takanabe, K. Kamata, X.C. Wang, M. Antonietti, J. Kubota, K. Domen, Phys. Chem. Chem. Phys. 12 (2010) 13020–13025.
- [12] S.X. Min, G.X. Lu, J. Phys. Chem. C 116 (2012) 19644–19652.
- [13] J.Y. Xu, Y.X. Li, S.Q. Peng, G.X. Lu, S.B. Li, Phys. Chem. Chem. Phys. 15 (2013) 7657–7665.
- [14] Y.B. Wang, J.D. Hong, W. Zhang, R. Xu, Catal. Sci. Technol. 3 (2013) 1703–1711.
- [15] D.H. Wang, Y.W. Zhang, W. Chen, Chem. Commun. 50 (2014) 1754–1756.
- [16] S. Ferrere, A. Zaban, B.A. Gregg, J. Phys. Chem. B 101 (1997) 4490–4493.
- [17] C. Huang, S. Barlow, S.R. Marder, J. Org. Chem. 76 (2011) 2386–2407.
- [18] L.I. Hernández, R. Godin, J.J. Bergkamp, M.J.L. Portolés, B.D. Sherman, J. Tomlin, G. Kodis, D.D. Méndez-Hernández, S. Bertolotti, C.A. Chesta, E. Marín~Ochoa, A.L. Moore, T.A. Moore, G. Cosa, R.E. Palacios, J. Phys. Chem. B 117 (2013) 4568–4581.
- [19] Y. Che, X.M. Yang, G.L. Liu, C. Yu, H.W. Ji, J.M. Zuo, J.C. Zhao, L. Zang, J. Am. Chem. Soc. 132 (2010) 5743–5750.
- [20] J.T. Kirner, J.J. Stracke, B.A. Gregg, R.G. Finke, ACS Appl. Mater. Interfaces 6 (2014) 13367–13377.
- [21] C. Li, H. Wonneberger, Adv. Mater. 24 (2012) 613–636.
- [22] E. Kozma, M. Catellani, Dyes Pigments 98 (2013) 160–179.
- [23] A. Senthilraja, B. Krishnakumar, M. Swaminathan, S. Nagarajan, New J. Chem. 38 (2014) 1573–1580.
- [24] L. Zang, Y. Che, J.S. Moore, Acc. Chem. Res. 41 (2008) 1596–1608.
- [25] S. Chen, D.L. Jacobs, J.K. Xu, Y.X. Li, C.Y. Wang, L. Zang, RSC Adv. 4 (2014) 48486–48491.
- [26] A.S. Weingarten, R.V. Kazantsev, I.C. Palmer, M. McClendon, A.P.S. Samuel, D.J. Kiebala, M.R. Wasielewski, S.I. Stupp, Nat. Chem. 6 (6) (2014) 964–970.
- [27] S. Chen, Y.X. Li, C.Y. Wang, RSC Adv. 5 (2015) 15880–15885.
- [28] A. Schwarzer, T. Saplinova, E. Kroke, Coord. Chem. Rev. 257 (2013) 2032–2062.
- [29] D.Q. Gao, Q. Xu, J. Zhang, Z.L. Yang, M.S. Si, Z.J. Yan, D.S. Xue, Nanoscale 6 (2014) 2577–2581.
- [30] Z.H. Hong, B. Shen, Y.L. Chen, B.Z. Lin, B.F. Gao, J. Mater. Chem. A 1 (2013) 11754–11761.
- [31] Y. Che, X.M. Yang, S. Loser, L. Zang, Nano Lett. 8 (2008) 2219–2223.
- [32] S.K. Choi, H.S. Yang, J.H. Kim, H. Park, Appl. Catal. B: Environ. 121–122 (2012) 206–213.
- [33] S.X. Min, G.X. Lu, Int. J. Hydrogen Energy 37 (2012) 10564–10574.
- [34] K. Balakrishnan, A. Datar, T. Naddo, J.L. Huang, R. Oitker, M. Yen, J.C. Zhao, L. Zang, J. Am. Chem. Soc. 128 (2006) 7390–7398.
- [35] K. Balakrishnan, A. Datar, R. Oitker, H. Chen, J.M. Zuo, L. Zang, J. Am. Chem. Soc. 127 (2005) 10496–10497.
- [36] C.C. Chen, W.H. Ma, J.C. Zhao, Chem. Soc. Rev. 39 (2010) 4206–4219.
- [37] Y.J. Zhang, T. Mori, L. Niu, J.H. Ye, Energy Environ. Sci. 4 (2011) 4517–4521.